Basic Astrophysical Concepts on Jetted AGN for the Lab high energy Session

OSSERVATORIO DI ASTROFISICA E SCIENZA DELLO SPAZIO

Paola Grandi

INAF-OAS paola.grandi @inaf.it
DIFA paola.grandi5@unibo.it

INAF ISTITUTO NAZIONALE DI ASTROFISICA OAS BOLOGNA

November 2025

Gamma Rays — Quick Overview

- Highest-energy photons in the electromagnetic spectrum
- Extremely short wavelengths (< 0.01 nm) and very high frequencies (> 10^{19} Hz)
- Energies > 10^5 eV (100 keV – TeV), up to **10^9×** an optical photon
- **HE (30 MeV – 100 GeV):** detected from space
- **VHE (100 GeV – 100 TeV):** detected with ground-based Cherenkov telescopes (IACTs)
- Trace **non-thermal**, **relativistic** processes and reveal sites of particle acceleration

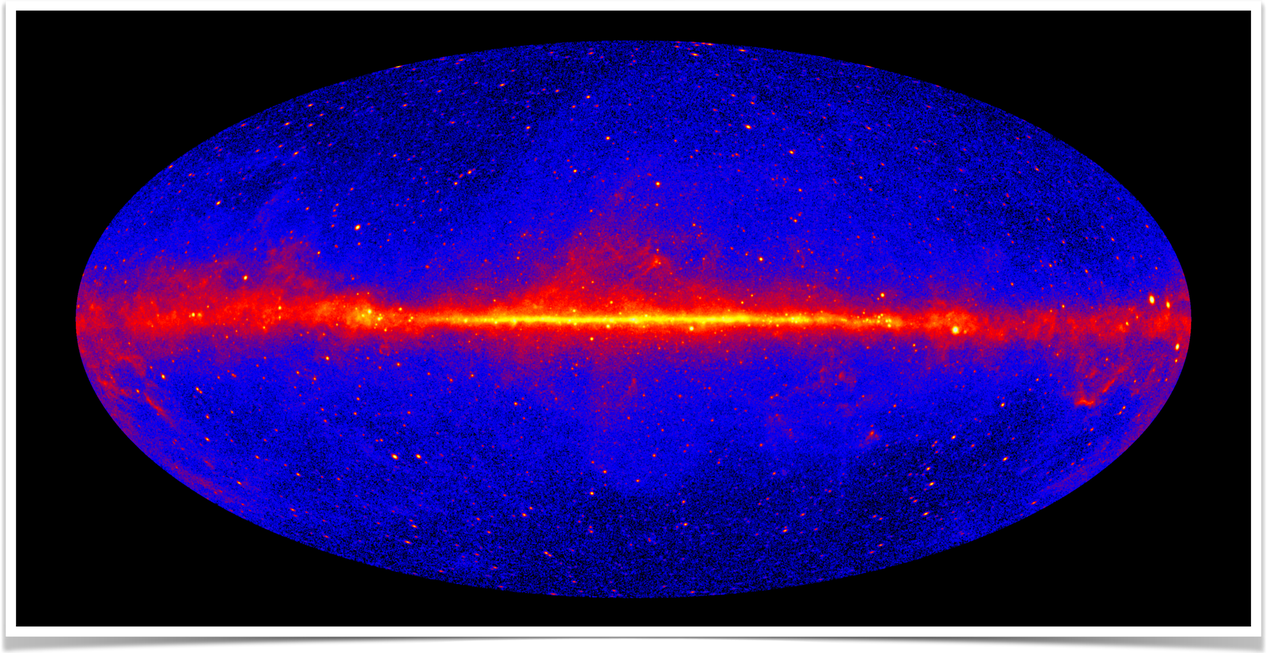

All-sky map from Fermi–LAT at energies > 1 GeV, obtained from 144 months of data

Challenges in Gamma-Ray Data Analysis Compared to X-Ray

- **X-ray**: Focused using mirrors and CCD detectors
- **X-ray**: Local background estimation from source-free regions
- **X-ray**: Sources studied in regions of a few arcseconds
- **X-ray**: Uses Gaussian statistics for photon counts.adding complexity.

- Gamma-ray: Cannot be focused; direction is through electron-positron pair conversion resulting in lower angular accuracy
- Gamma-ray: Requires global background modeling, considering Galactic diffuse emission, isotropic emission, and all point sources in the Region of Interest (ROI)
- Gamma-ray: Sources studied in regions spanning several degrees due to broader point-spread function (PSF)
- Gamma-ray: Poisson likelihood needed due to low photon counts and multi-dimensional data, adding complexity

Count map

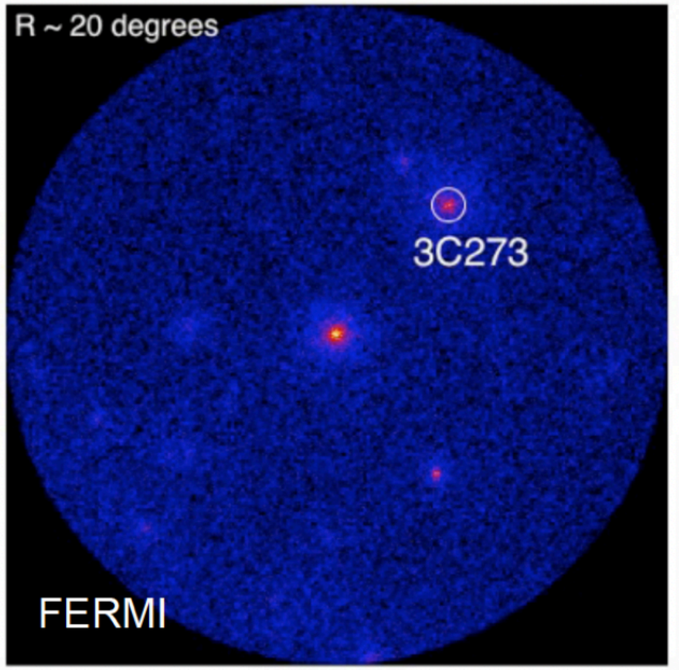
R ~ 20 degrees
3C273
FERMI


10
20
30
40
50

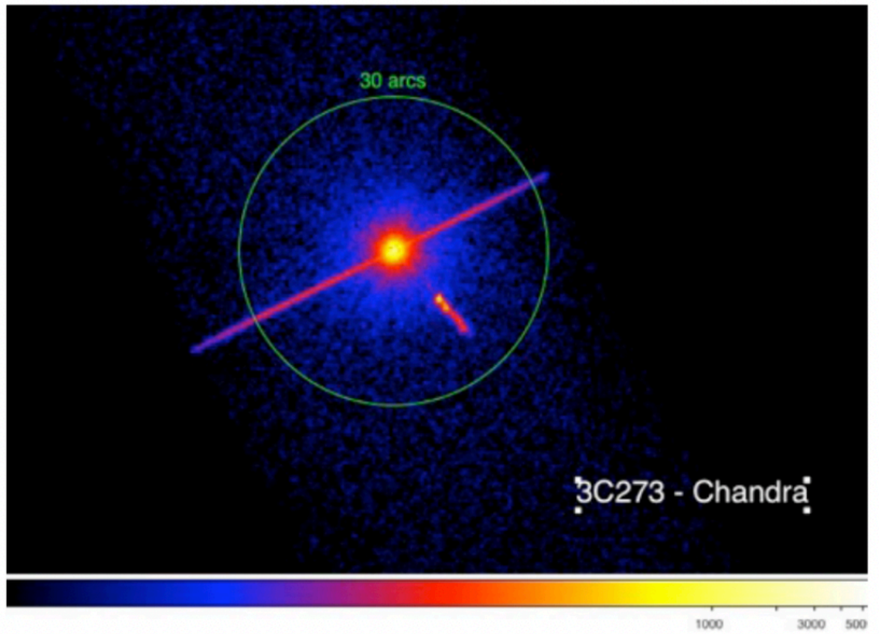
30 arcs
3C273 - Chandra
1000
3000
500

The gamma-ray sky is dominated by two main classes of sources: **blazars and pulsars**

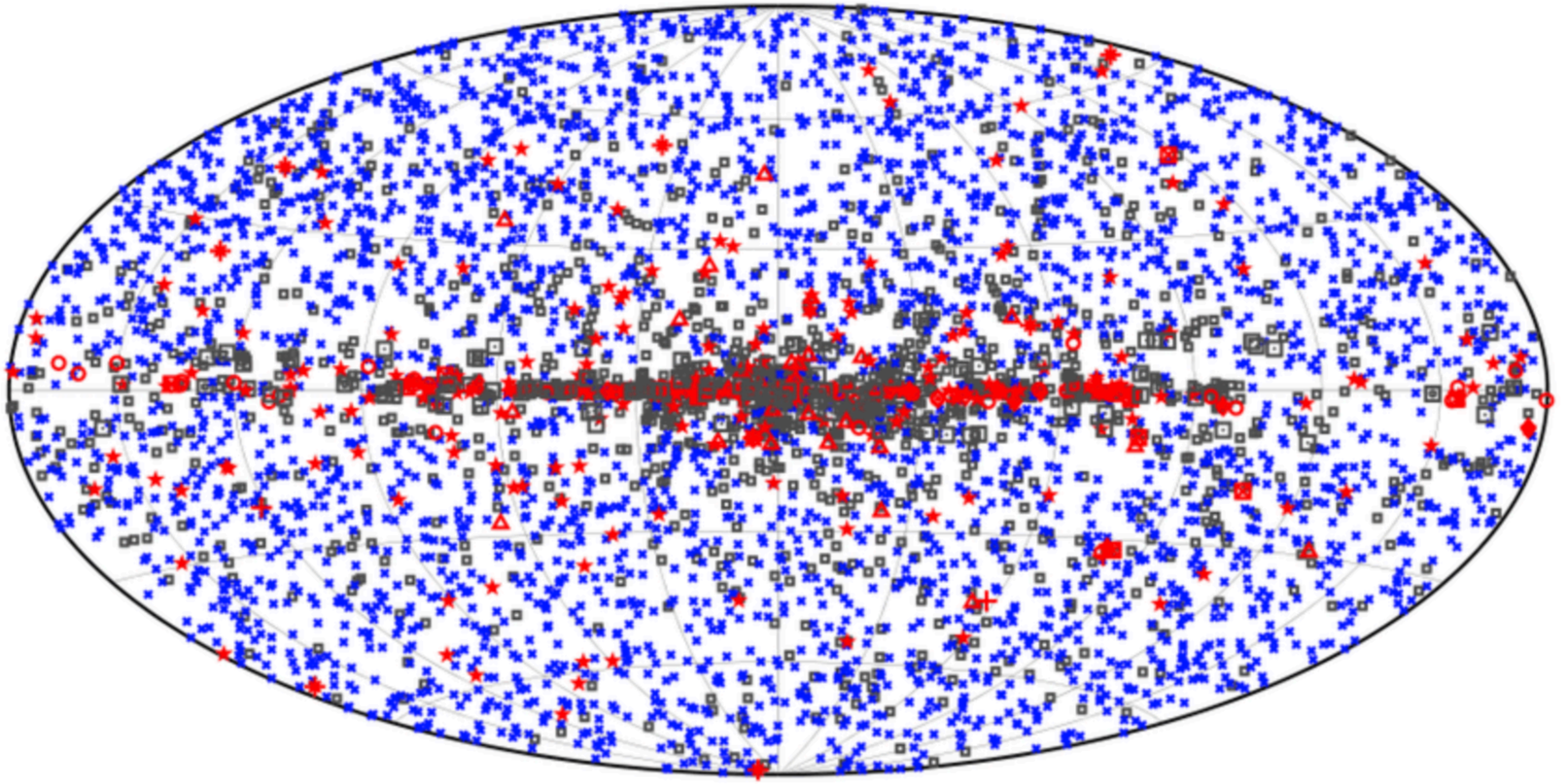

FGL = *Fermi Gamma-ray LAT catalog*

No association	Possible association with SNR or PWN		AGN
Pulsar	Globular cluster	Starburst Galaxy	PWN
Binary	Galaxy	SNR	Nova
Star-forming region	Unclassified source		

The Fermi-LAT team regularly updates its source catalogs (from 1FGL and 2FGL to the latest 4FGL-DR1–DR4 versions)

The object studied in this laboratory test is
an active galaxy emitting a relativistic plasma jet pointing towards us

Most galaxies are known to host a central supermassive black hole

but only about 1% show an Active Galactic Nucleus (AGN

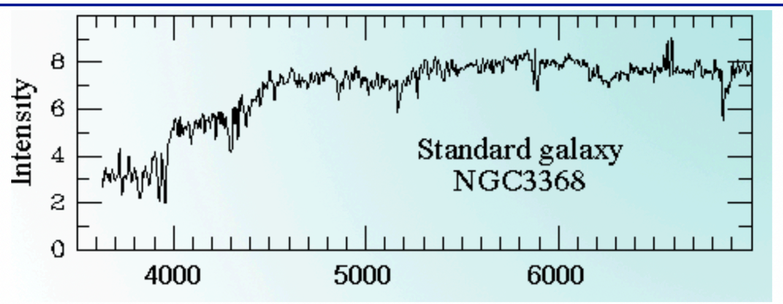

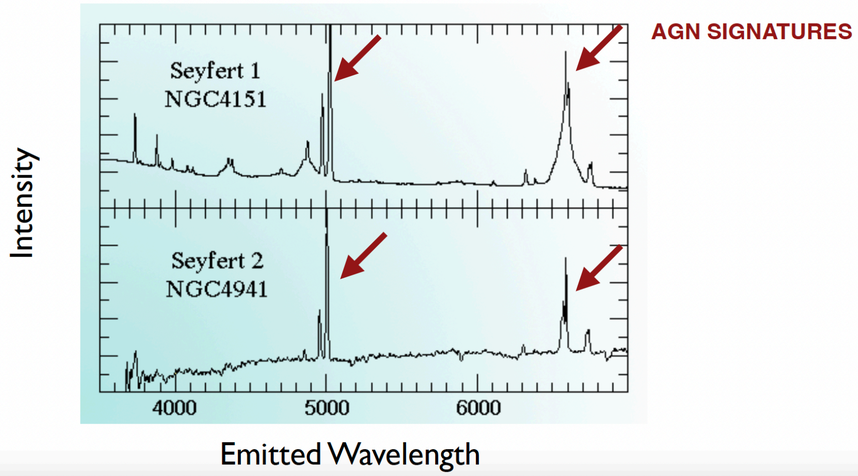

AGN SIGNATURES

AGN engine occupies a tiny region in the center of the galaxy

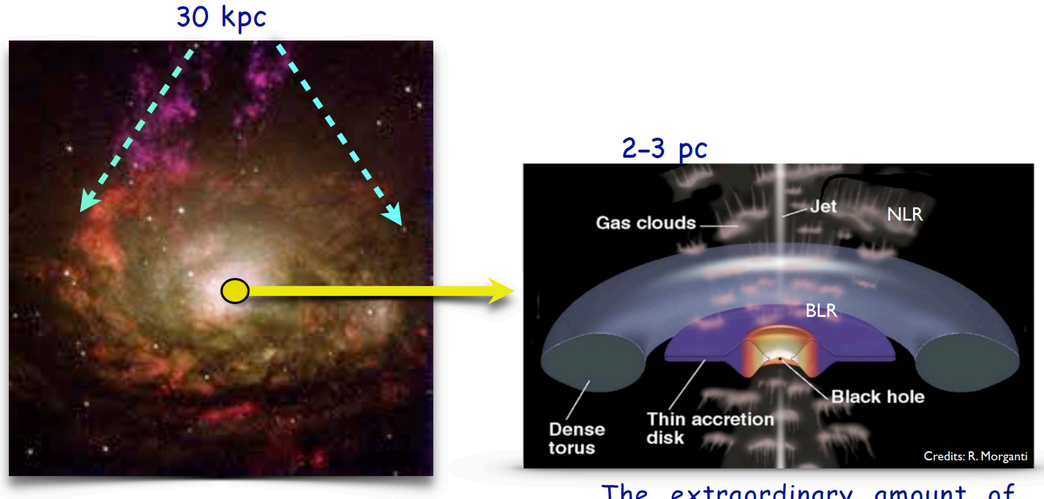

The extraordinary amount of energy is produced through accretion of gas close to a SMBH

About 10% of AGN are Radio-Loud,
i.e. these systems can launch relativistic jets

RL AGN lie in ellipticals
RQ AGN lie in spirals and ellipticals

The central engine of an AGN is powered by matter accreting onto a supermassive black hol

Accretion processes around black holes involve rotating gas flow. Therefore the accretion flow structure is determined by solving simultaneously four conservation equations:

conservation of vertical momentum
conservation of mass
conservation of energy
conservation of angular momentum

Four solutions are currently known. In these solutions viscosity transports angular momentum outward, allowing the accretion gas to spiral in toward the BH. Viscosity acts a source of heat that is radiated away.

The most famous solutions are:

i) Shakura & Sunyaev thin optically thick disk model (standard model)

ii) Optically thick Advection-Dominated Accretion Flow (ADAF)

How the Shakura–Sunyaev Disk Works

A Shakura–Sunyaev disk is geometrically thin and optically thick

- Gas spirals inward because turbulence and magnetic stresses transport angular momentum outward
- Moving inward, the gas loses gravitational energy, which is dissipated as heat
- This heat is radiated locally, producing a multi-temperature blackbody spectrum
- The viscosity that drives accretion is described by the α-parameter.

Thin $H/R << 1$

Optically thick disk => radiation and matter are in thermal equilibrium
the disk emits locally like a black body

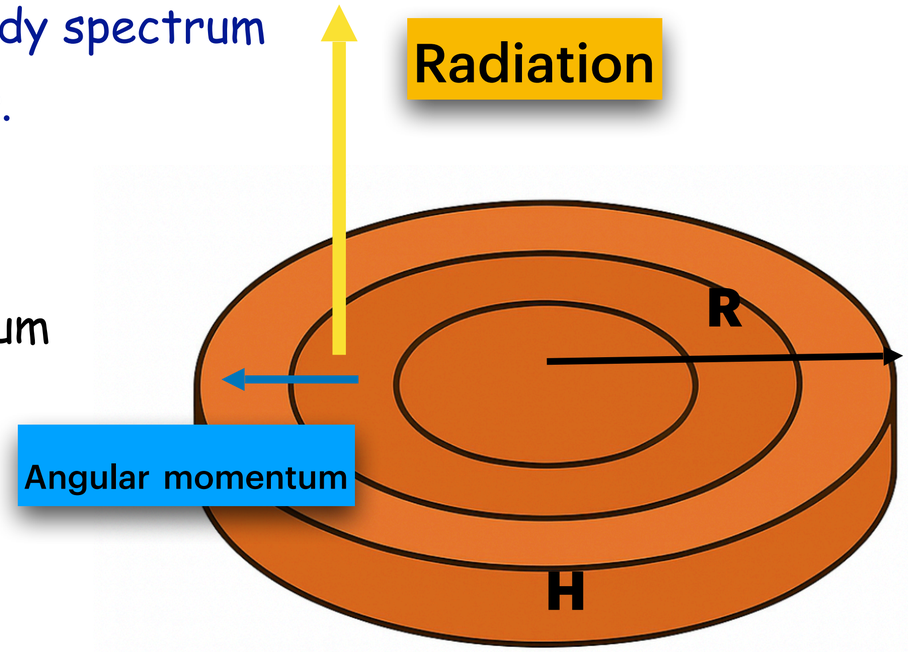

How the ADAF Works

In this solution the accreting gas has a very low density and is unable to cool efficiently. The viscous energy is stored in the gas as thermal energy instead of being radiated and is advected onto the BH. Ions and electrons are thermally decoupled.

- Very Hot: Ti~ 10^{12}K (R_S/R), Te~ $10^{9\text{-}11}$K (since ADAF loses very little heat).

- Geometrically thick: H~R (most of the viscosity generated energy is stored in the gas as internal energy rather than being radiated, the gas puffes up

- Optically thin (because of low density)

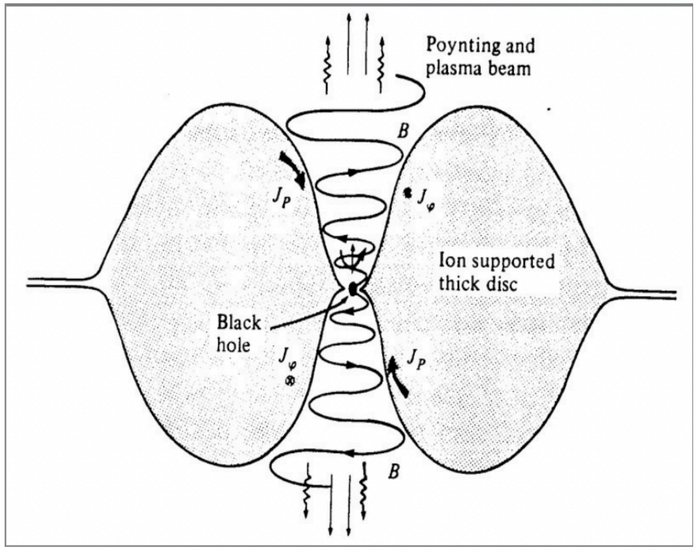

Accretion Regimes

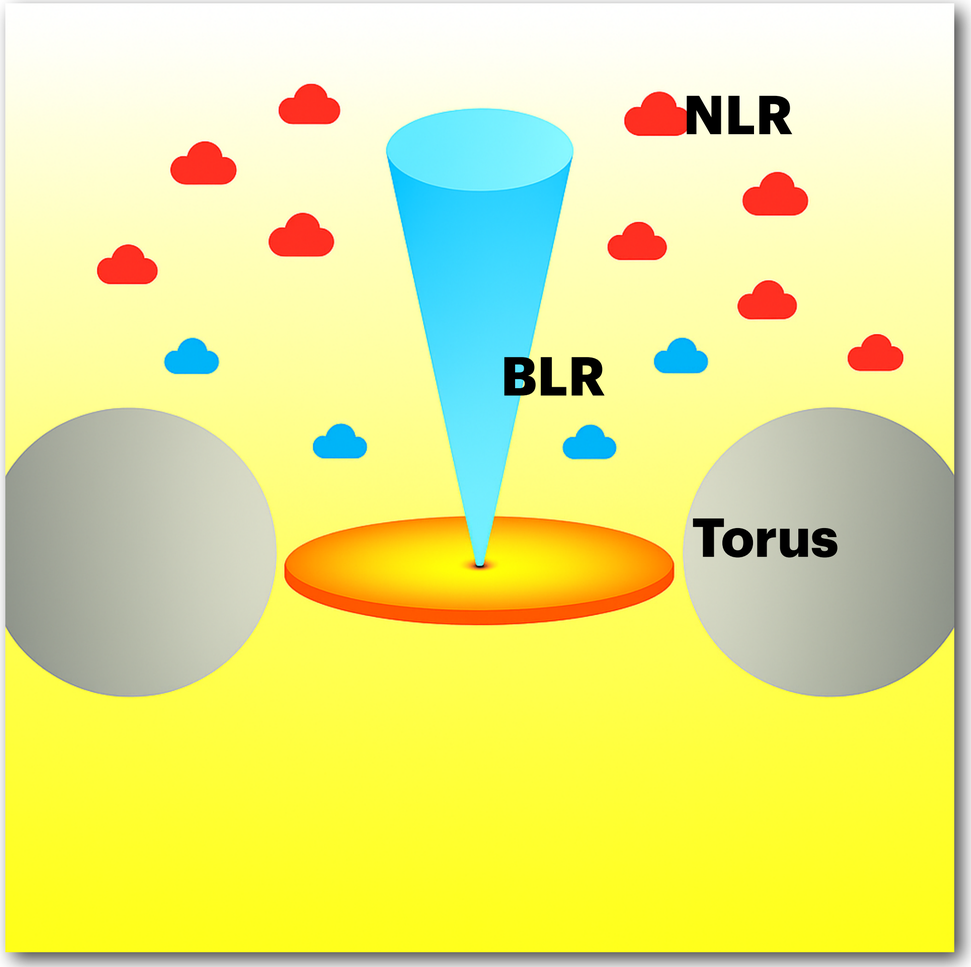

Efficient Accretion disk

Photon-rich and matter-rich environment

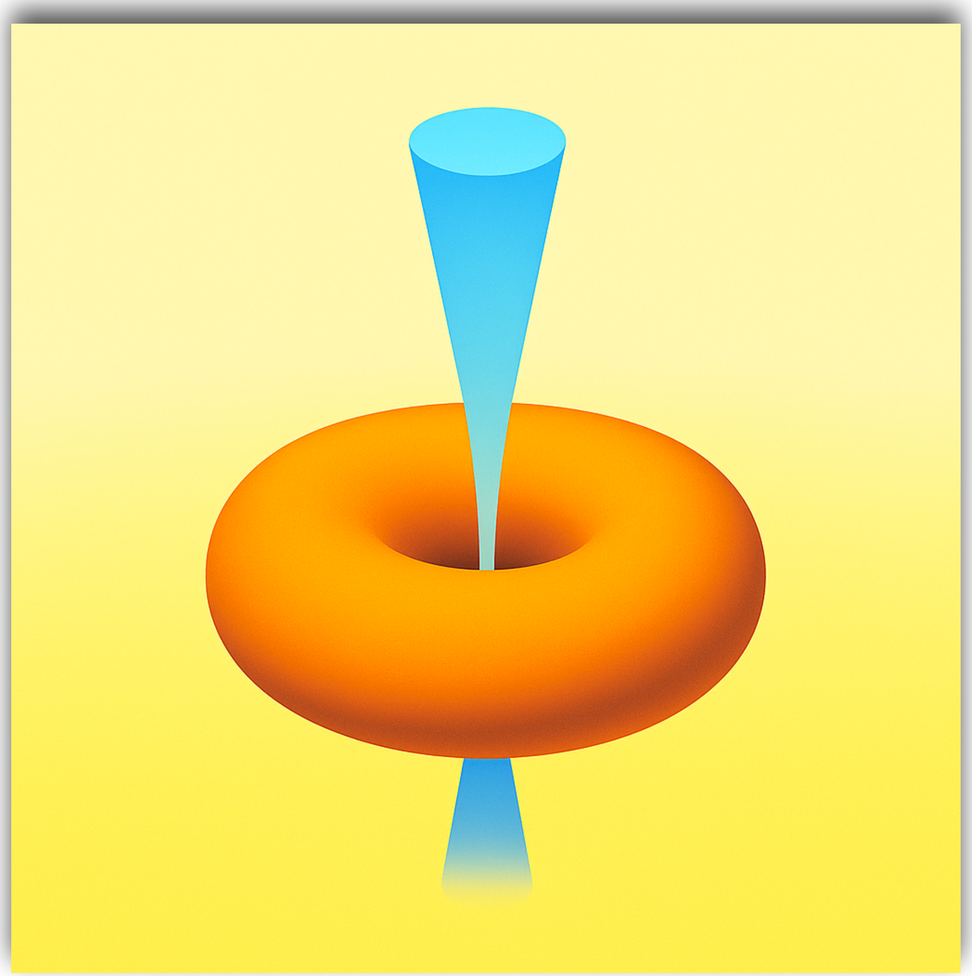

Inefficient flow -ADAF

Photon-poor environment

Schematic view (not to scale

How AGN Jets Are Launched – Simple Points

- The accretion flow brings a poloidal (vertical) magnetic field toward the black hole.
- In plasma, the magnetic field is "frozen-in," so the inflowing gas drags the field lines inward.
- A spinning black hole drags spacetime around it (frame dragging).
- This rotation twists the vertical (poloidal) magnetic field lines.

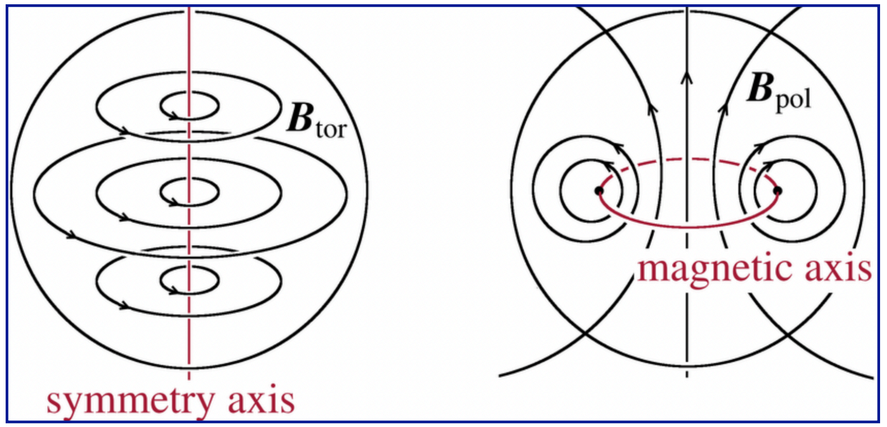

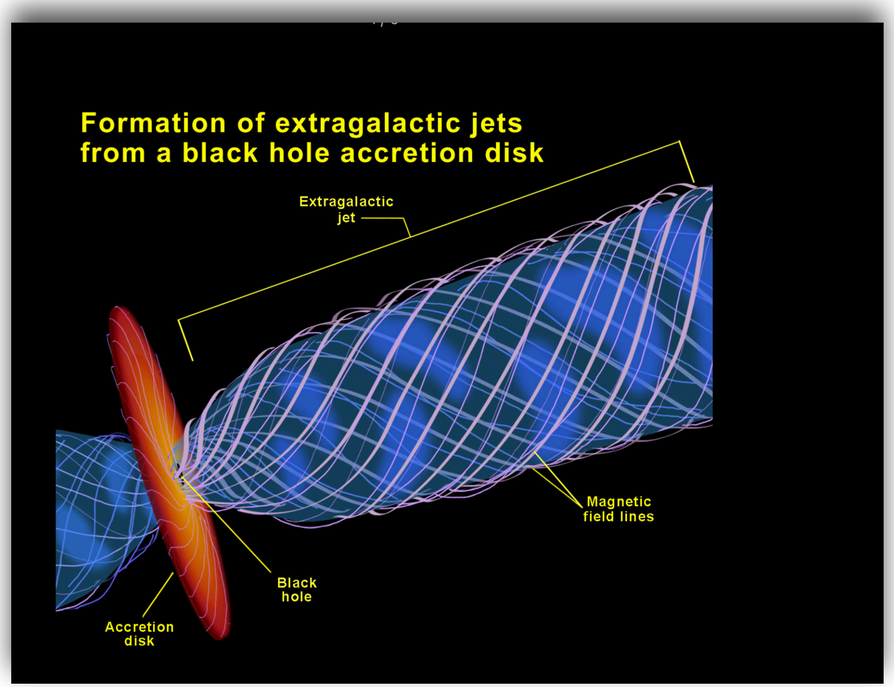

- Twisting generates a strong toroidal (azimuthal) magnetic field Btor.
- The toroidal field has high magnetic pressure ($\propto$ Btor^2).
- This magnetic pressure pushes energy and plasma outward along the rotation axis.
- Plasma moves along the magnetic field lines $\rightarrow$ a narrow, collimated jet forms.
- The jet is powered by the rotational energy of the black hole.

The jet emission is strongly Doppler boosted

The key parameter is the Doppler Factor $\delta(\beta, \theta)$

$$\delta = [\gamma(1 - \beta \cos\theta)]^{-1}$$

Lorentz factor $\gamma = \frac{1}{\sqrt{(1-\beta^2)}}$

$\beta = \frac{v}{c}$ **, V-> jet bulk motion**

Angle between the jet and the observer

The Doppler factor relates intrinsic and observed flux for a moving source at relativistic speed v=β c.

For an **intrinsic** power law spectrum: $F'(\nu') = K (\nu')^{-\alpha}$
the **observed** flux density is

$$F_\nu(\nu) = \delta^{3+\alpha} F'_{\nu'}(\nu)$$

The Doppler factor reduces the time by a factor $1/\gamma$

$$\Delta t = \Delta t'/\delta$$

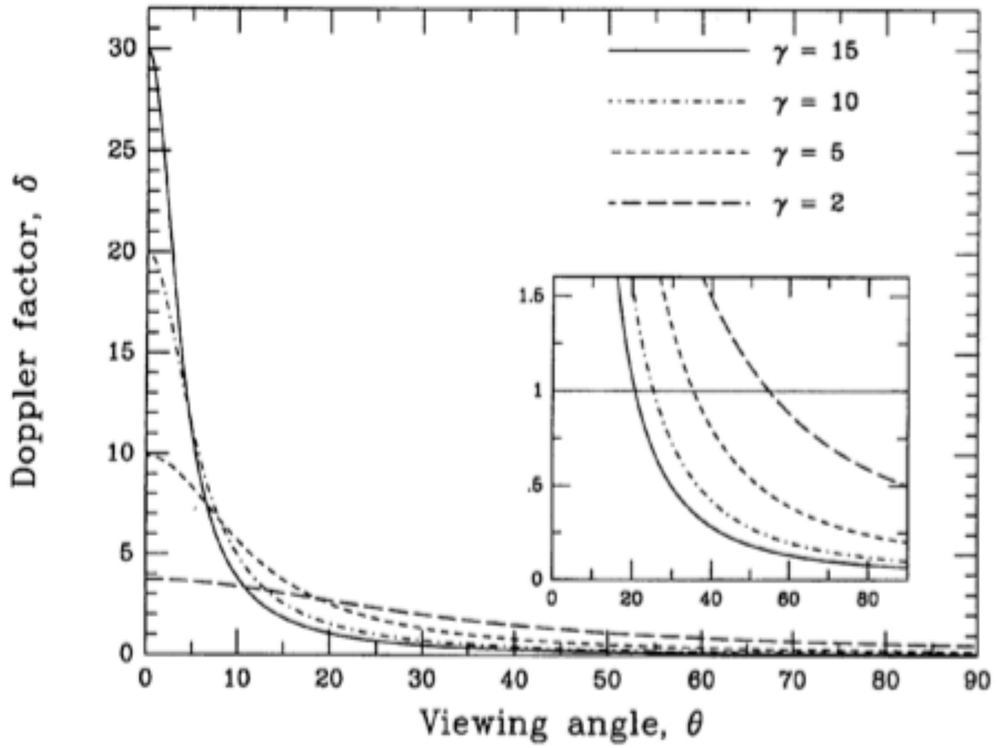

Blazars: BL Lacs (BL) and Flat Spectrum Radio Quasar (FSRQ)

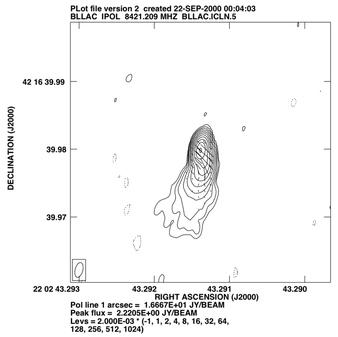

Compact in radio

BL are almost featureless in the optical band (FSRQ can show emission lines overimposed on a strong continuum)

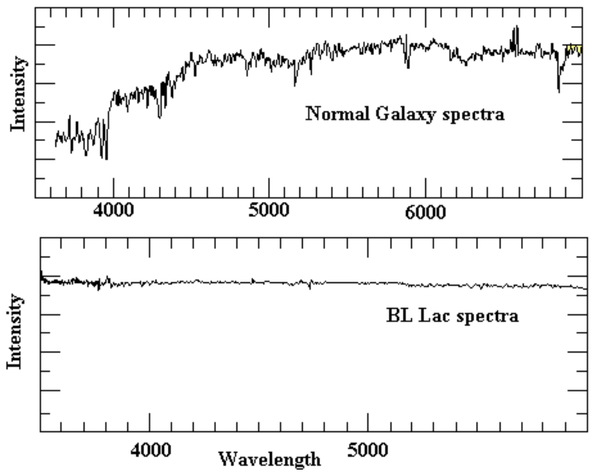

Extremely variable

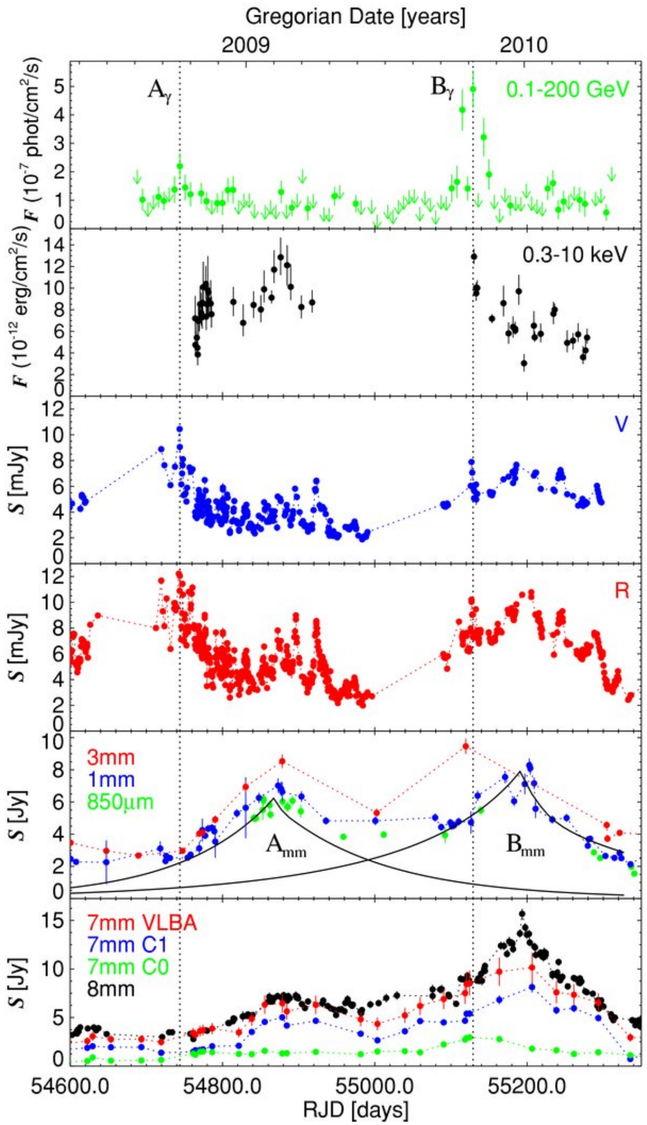

OJ 287 light curves from radio to gamma

Agudo et al. 2011ApJL 726, L13

When the jet is the dominant component:AGN are classified as BL LAC or Flat Spectrum Radio Quasars

ADAF

Sakura-Sunyaev disc

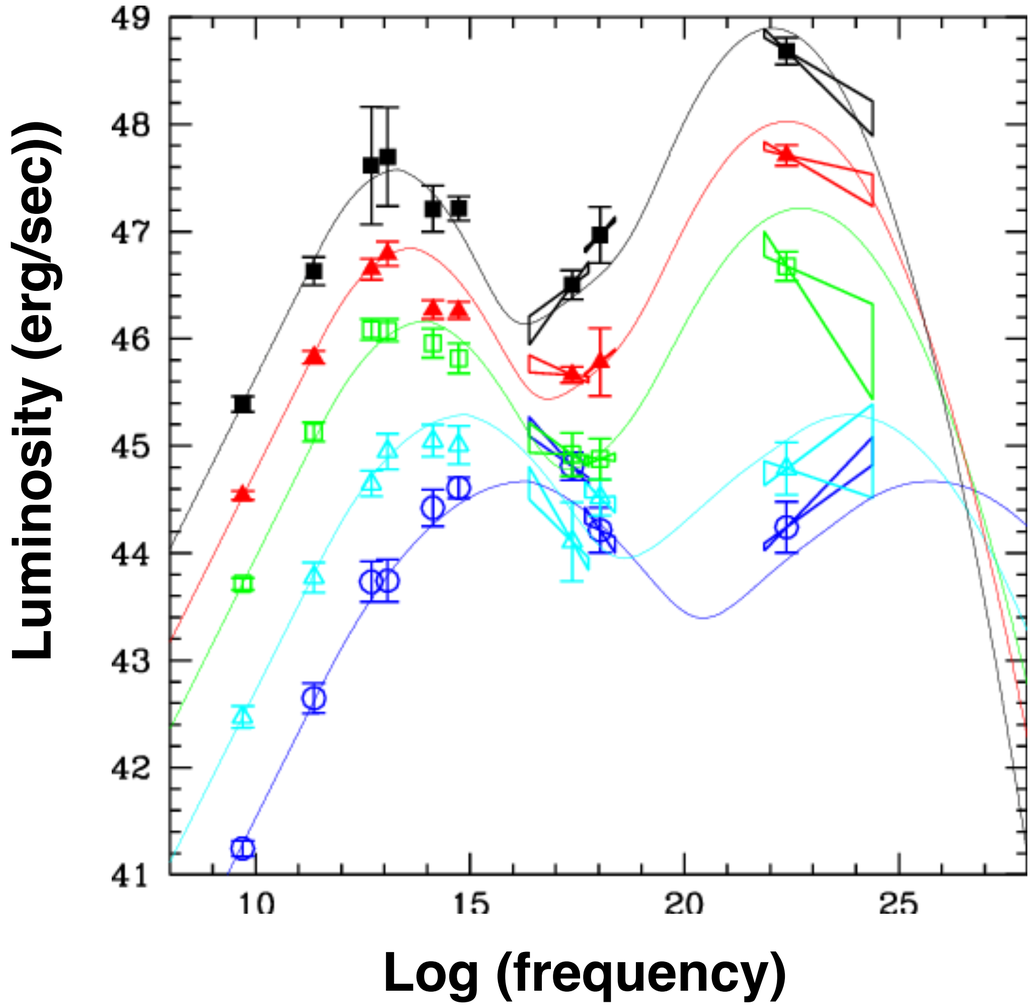

BLAZARS: double peaked SED

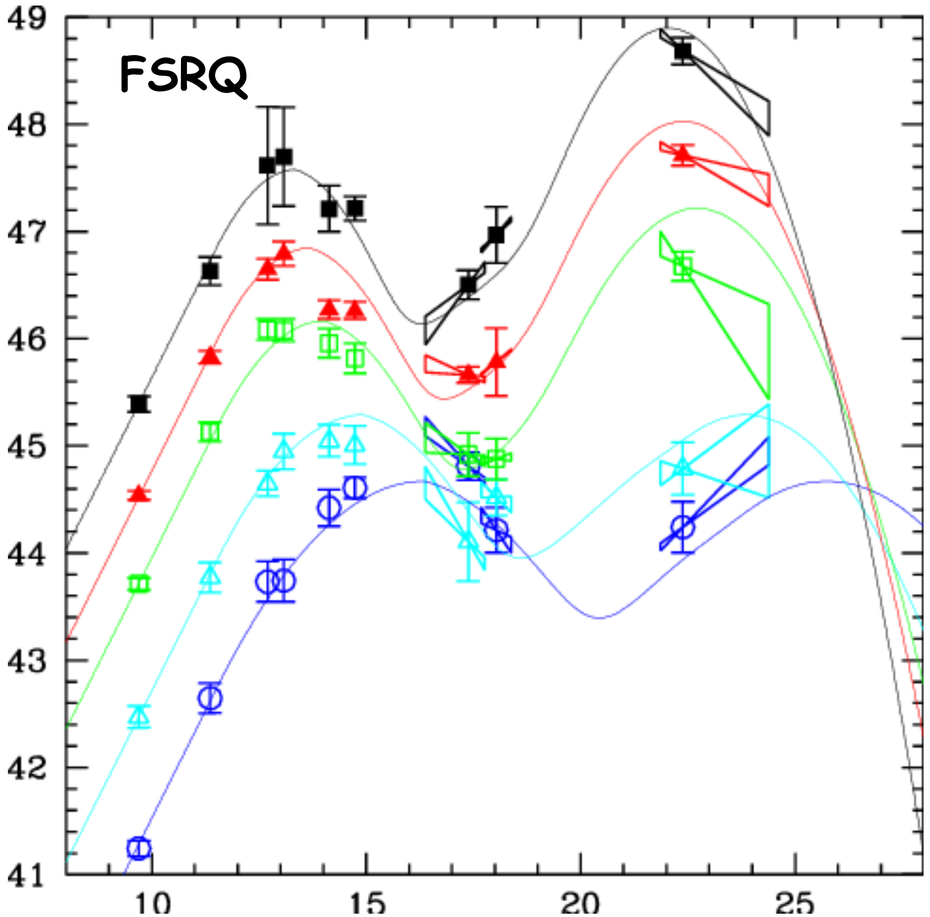

LBL (Low-frequency-peaked BL Lacs):
Synchrotron peak at lower frequencies

IBL (Intermediate BL Lacs):
Synchrotron peak at intermediate frequencies

HBL (High-frequency-peaked BL Lacs):
Synchrotron peak at higher frequencies.

double peaked SED
(Fossati et al. 1998)

Synchrotron Radiation

Synchrotron radiation is due to the movement of an electron charge in a magnetic field. As a particle gyrates around a magnetic field, it will emit radiation at a frequency proportional to the strength of the magnetic field and its velocity.

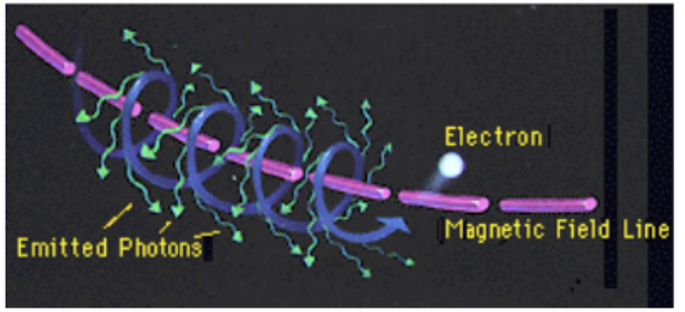

Synchrotron radiation is highly polarized and is seen at all wavelengths. At relativistic speeds, the radiation can also be beamed. It is very common in radio spectrum, but can be seen in x-rays. It is usually fit as a power law. For full details, see the review by Ginzburg & Syrovatskii (1969)

The synchrotron radiation of a power law distribution of electron energies

Synchrotron

$$N(\gamma_e) = K\gamma_e^{-p}, \quad \gamma_{min} < \gamma_e < \gamma_{max}, \; p = 1 + 2\alpha$$

$$\epsilon_{sin}(\nu) \propto KB^{\alpha+1}\nu^{-\alpha} \quad \text{erg cm}^{-3}\,\text{s}^{-1}\,\text{sr}^{-1}$$

Inverse Compton scattering

When the electron is not at rest, but has an energy greater that the typical photon energy, there can be a transfer of energy from the electron to the photon. This process is called Inverse Compton to distinguish it from the direct Compton scattering, in which the electron is at rest, and it is the photon to give part of its energy to the electron.

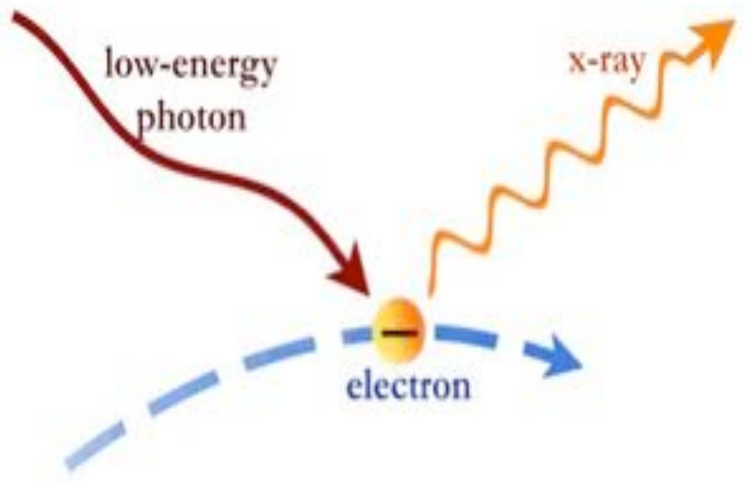

$$< \nu >= \frac{4}{3}\gamma^2 \nu$$

Inverse Compton radiation of a power law distribution of electron energies

$$N(\gamma_e) = K\gamma_e^{-p}, \quad \gamma_{min} < \gamma_e < \gamma_{max}, p = 1 + 2\alpha$$

Inverse Compton

$$\epsilon_c(\nu_c) \propto K\nu_c^{-\alpha} \int \frac{Ur(\nu)\nu^{\alpha}}{\nu} d\nu$$

erg cm^{-3} s^{-1} sr^{-1}

U_r is the radiation energy density

$$U_r = \int n(\epsilon)\epsilon d\epsilon$$

- **Synchrotron photons in the jet**
- Environment photons from Accretion Flow, BLR, NLR, Torus
- Cosmic Microwave Background (CMB) photons

Self Synchrotron Model —>
Synchrotron photons in the jet are up scattered to higher energies

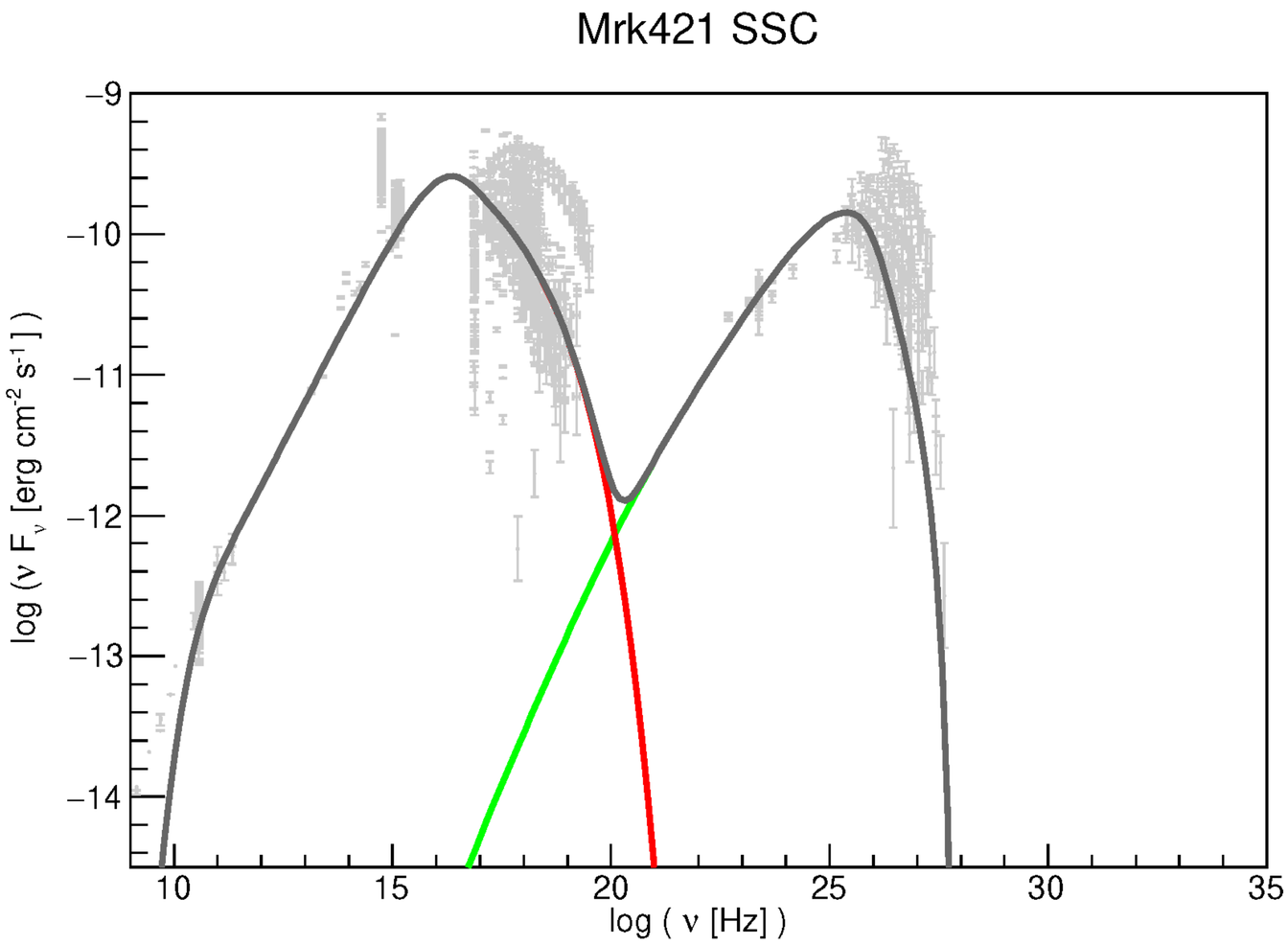

Bronzini PhD thesis 2025

External Compton Model —>

Synchrotron photons in the jet + **Environment photons from Accretion Flow, BLR, NLR,Torus are up scattered to higher energies**

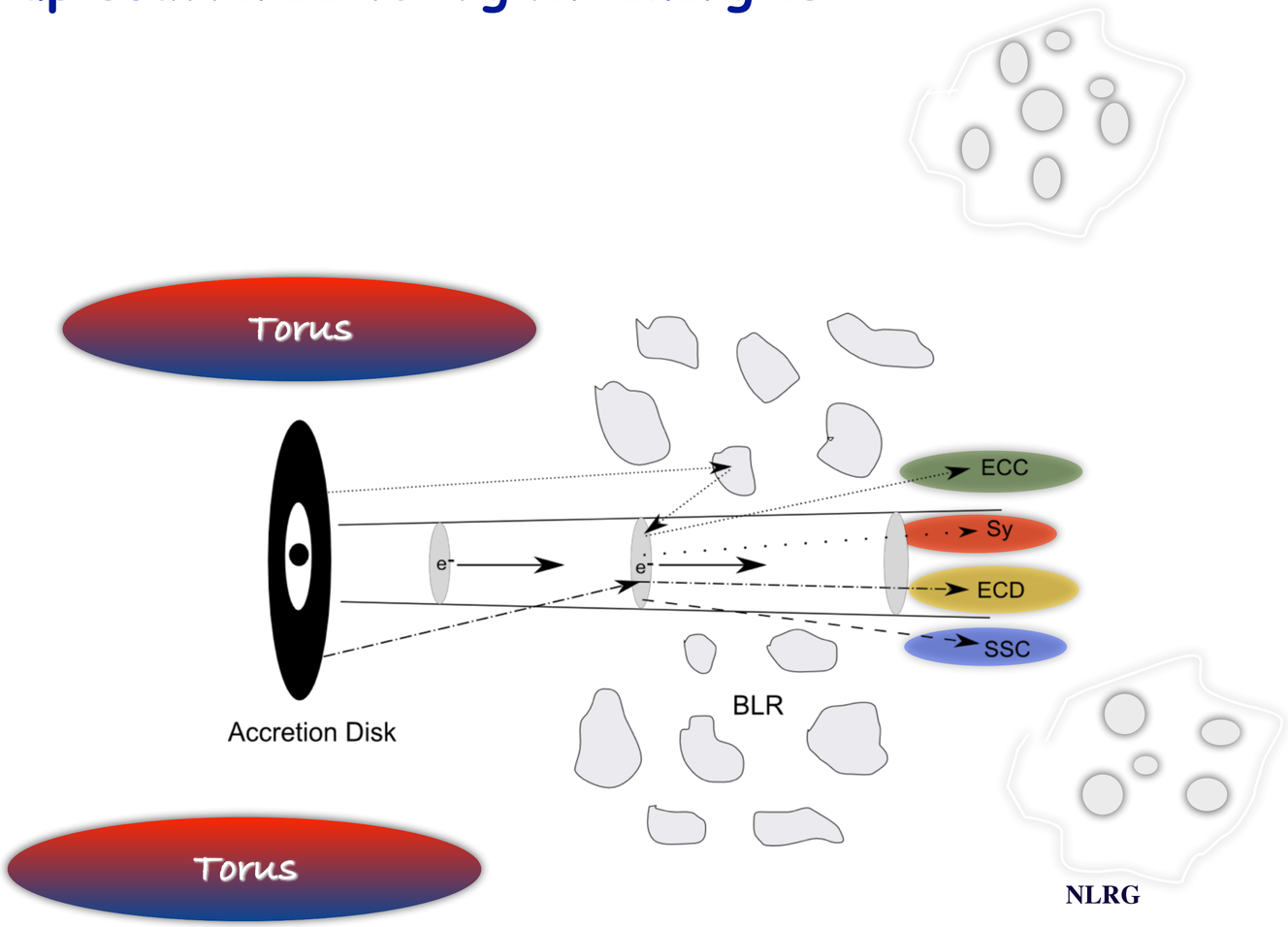

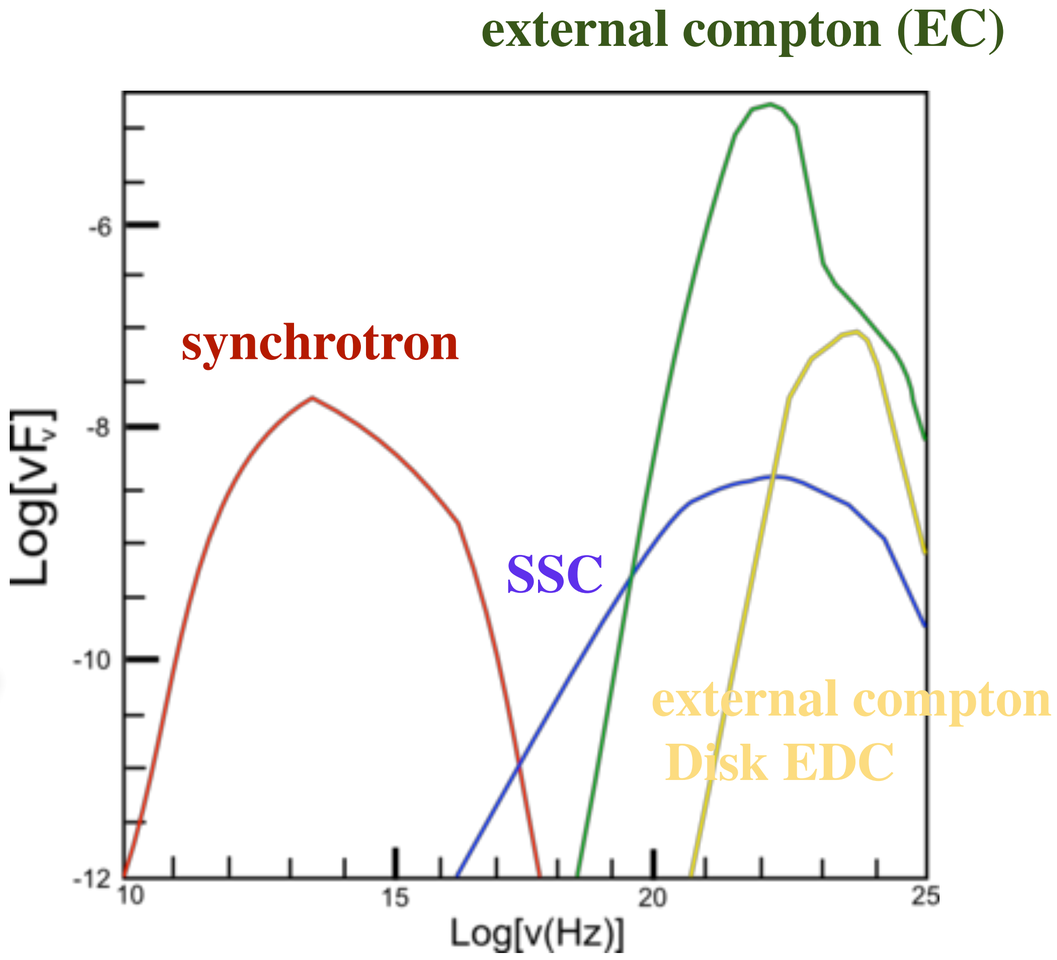

Hadronic Models and Neutrinos

High energy SED peack

- Can be explained by **hadronic models**.
- Dominant emission mechanism: **proton synchrotron**.

$$
\begin{aligned}
&\mathrm{p} + \gamma \rightarrow \mathrm{p}' + \pi^0 && \pi^0 \rightarrow 2\gamma \\
&\rightarrow \mathrm{n} + \pi^+ && \pi^+ \rightarrow \mu^+ + \nu_\mu \rightarrow \mathrm{e}^+ + \nu_\mathrm{e} + \overline{\nu}_\mu + \nu_\mu \\
&\rightarrow \mathrm{p}' + \pi^+ + \pi^- && \pi^- \rightarrow \mu^- + \overline{\nu}_\mu \rightarrow \mathrm{e}^- + \overline{\nu}_\mathrm{e} + \nu_\mu + \overline{\nu}_\mu \\
&\mathrm{p} + \gamma \rightarrow \mathrm{p}' + \mathrm{e}^- + \mathrm{e}^+.
\end{aligned}
$$

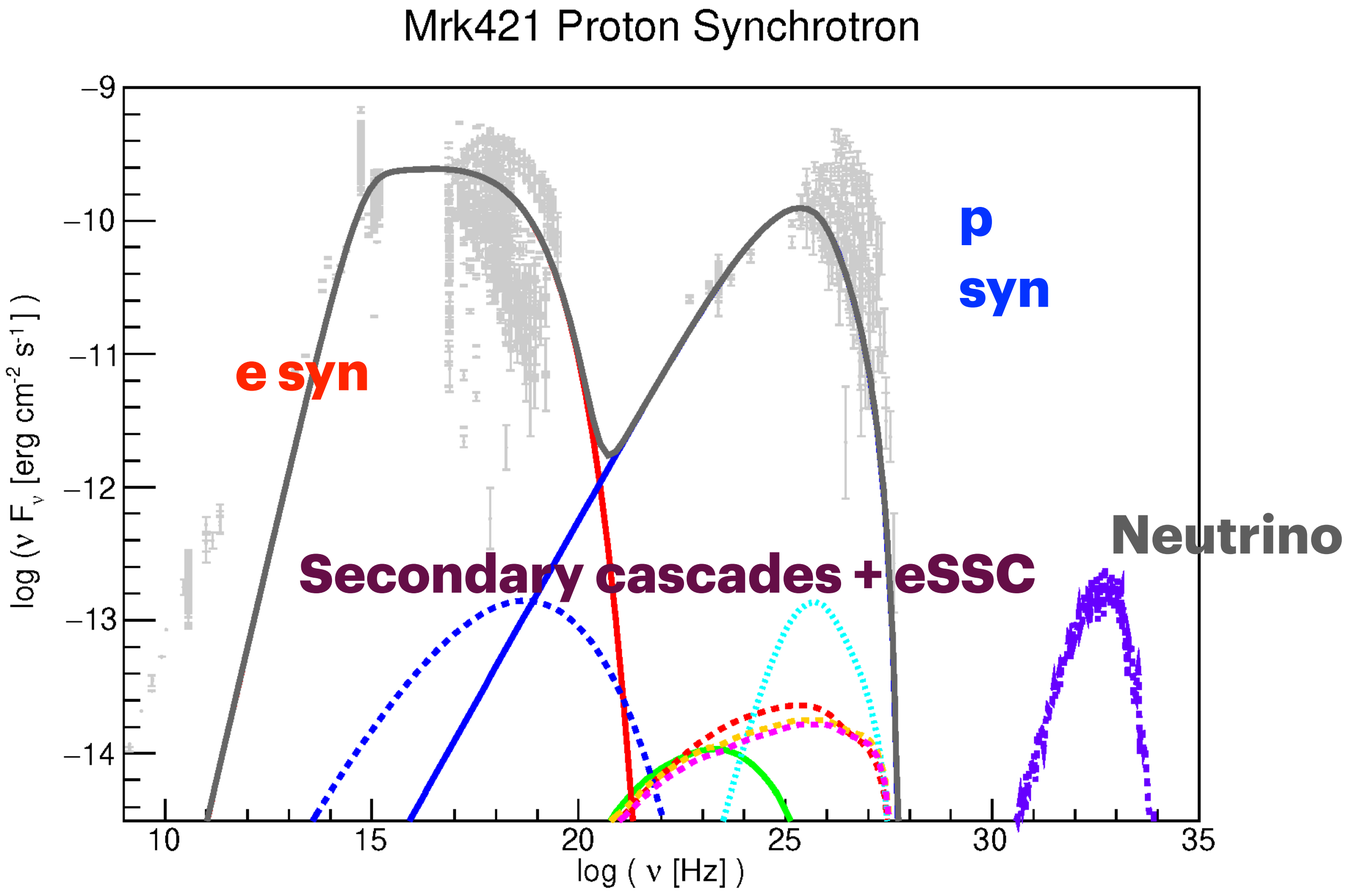

Bronzini PhD thesis 2025

Exercise: Data Analysis and Reduction for TXS0506+56

Mandatory

- Understand **every single step** in the data reduction process.
- The **main input parameters** must be fully understood, as well as the structure of both **input** and **output files**.

These topics will be part of the exam

- **Data Reduction with Fermi**:
  - Process Fermi data for the source TXS0506+56 using Jupyter Notebook.

- **Spectral Energy Distribution (SED)**:
  - Construct the FERMI -LAT SED for the source.

- **Light Curves**:
  - Construct one or more light curves to track the variation in flux over time.

Optional

1. Build a SED from radio to TeV

- The radio to X-ray data will be provided already in units of erg/s/cm^2.
- The Fermi flux points are from your analysis
- The TeV flux points will be provided, but not in unit of erg/s/cm^2

2. Estimate an upper limit on the size of the region responsible for the gamma-ray flare and neutrino production

- Use the causality principle
- Consider the flux doubling time
- Verify that the flux difference between the points considered is statistically significant ($\geq 3\sigma$).

The Fermi satellite

Launched on 11 June 2008, it is still operational after more than 15 years in orbit.

The LAT operates mostly in survey mode, where it continuously scans the whole sky covering the entire sky every 3 hours.

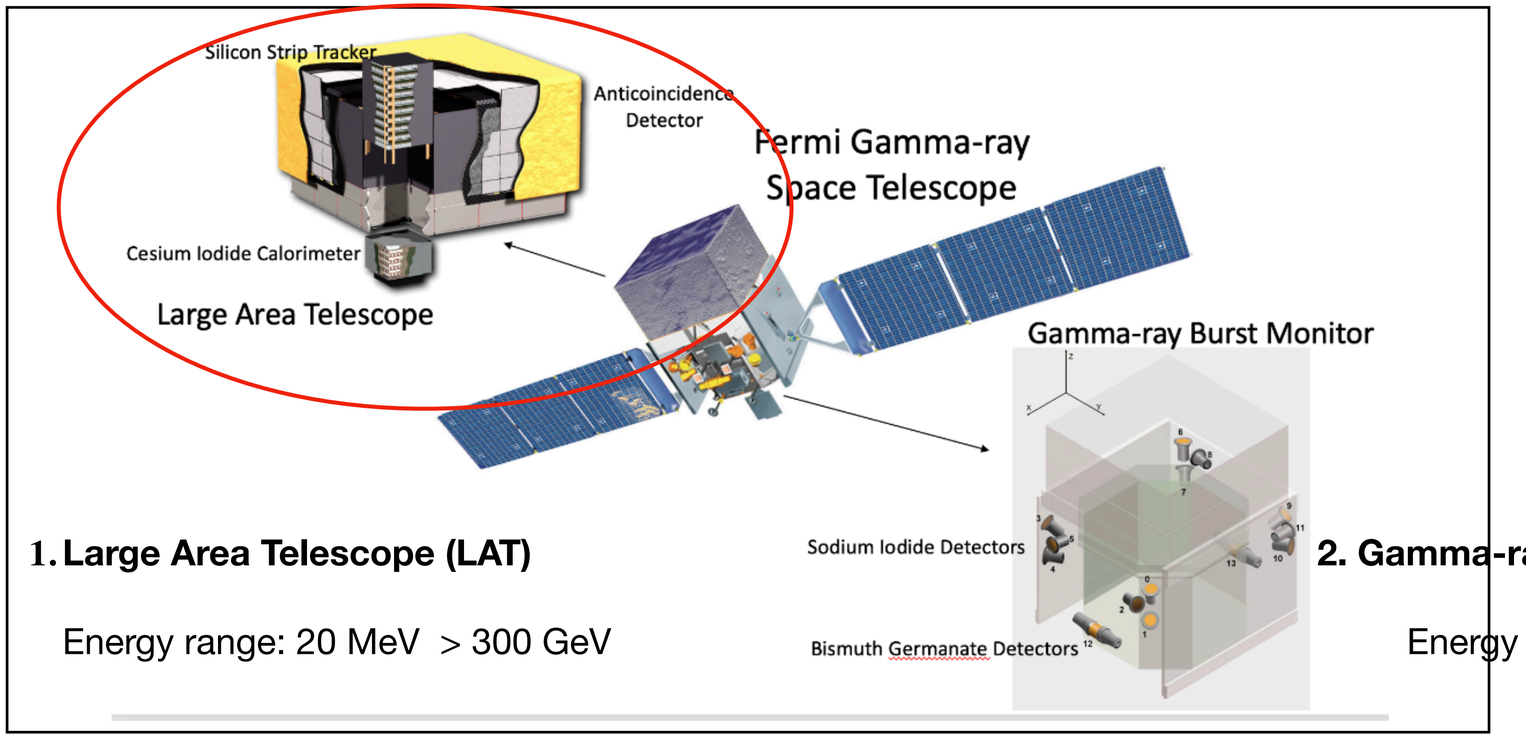

1. **Large Area Telescope (LAT)**

   Energy range: 20 MeV > 300 GeV

2. **Gamma-ray Burst Monitor (GBM)**

   Energy range: 8 keV – 40 MeV

LARGE AREA TELESCOPE

LAT is composed of **16 identical towers** arranged in a **4 × 4 array**.

Each tower includes three main subsystems:

- **Tracker (TKR)**
- **Calorimeter (CAL)**
- **Anticoincidence Detector (ACD)**

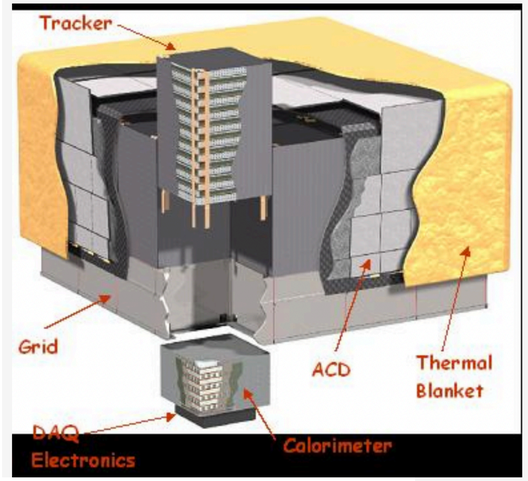

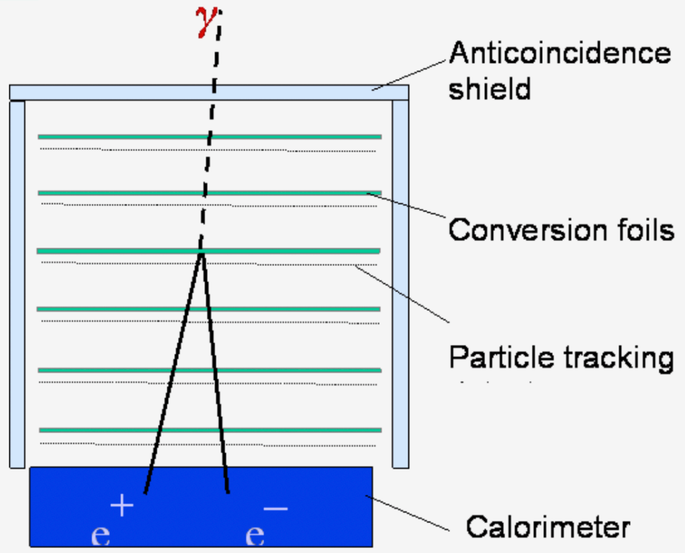

LAT Tracker (TKR)

- Built with alternating layers of thin tungsten foils and silicon strip detectors.
- Pair production occurs in the tungsten: the high atomic number (Z=74) provides high conversion efficiency ($\sigma_{pair} \propto Z^2$)
- The silicon planes measure the tracks of the electron–positron pair, allowing reconstruction of the incoming gamma-ray direction.
- Two regions:
  - Front section: thin tungsten → better angular resolution.
  - Back section: thick tungsten → better effective area

Calorimeter (CAL)

- Made of CsI(Tl) scintillating crystals. Charged particles ionize each crystal layer, producing light ‘tracks’ that build a 3D image of the shower.
- The total scintillation light is proportional to the deposited energy
- The shower shape
  - helps correct energy leakage due to particles escaping the calorimeter.
  - provides background discrimination: EM showers (photons/electrons) are compact, while Hadronic showers (protons/nuclei) are broader and irregular

Anticoincidence Detector (ADC)

outer shield covering the top and sides of the instrument. It rejects charged cosmic-ray particles (protons, electrons) entering the detector.

Event classification

The raw information transmitted by the Fermi satellite is called Level 0 data.
On the ground, these data undergo a first processing stage that produces Level 1 data
Level 1 **is the starting point for all LAT scientific analysis.**

Level 0 → Level 1: LAT Processing Steps

- **Interaction reconstruction**
  Rebuilds the particle's path
- **Event identification**
  Distinguishes true gamma rays from cosmic-ray background.
- **Physical characterization**
  Determines photon direction, energy, and other key parameters for analysis.

The Fermi satellite

FERMI (gamma) vs XMM-Newton (X)

Unlike optical light and X-rays, gamma rays cannot be focused or reflected by mirror

Gamma-ray instruments (LAT) exploit pair production, a process that occurs only at high energies

The incoming γ photon is converted into matter, producing an electron–positron pair: $\gamma \rightarrow e^+ + e^-$

The photon must have at least 1.022 MeV (twice the electron rest mass) to produce a pair

Each detected event is classified according to
its probability of being a true astrophysical photon and the quality of its reconstruction

These criteria define event classes (pass P8R3)
each class is associated with its own Instrument Response Functions (IRFs),

Event Class	Hierarchy	evclass	Description / Main Use
P8R3_TRANSIENT020	Standard	16	Transient event class with background rate ∼ 2×A10 IGRB, being A10 IGRB the isotropic gamma-ray background (IGRB) intensity defined in the Ackermann et al. (2010) model. Used for short-duration phenomena (GRBs, flares) where maximizing photon counts is essential.
P8R3_TRANSIENT010	Standard	64	Transient event class with background rate comparable to A10 IGRB. Suitable for bright, short events.
P8R3_SOURCE	Standard	128	Recommended for most analyses. Balanced between purity and photon statistics; ideal for point-like or moderately extended sources.
P8R3_CLEAN	Standard	256	Identical to SOURCE below 3 GeV, but with 1.3–2× lower background above 3 GeV. Suitable for high-latitude and hard-spectrum sources.
P8R3_ULTRACLEAN	Standard	512	Very low background and excellent PSF. Similar background rate to ULTRACLEANVETO; suited for diffuse studies.
P8R3_ULTRACLEANVETO	Standard	1024	The cleanest Pass 8 event class. Background ∼15–20% lower than SOURCE below 10 GeV and ∼50% lower at 200 GeV. Best for diffuse or low-background studies.
P8R3_SOURCEVETO	Standard	2048	Similar to SOURCE below 10 GeV; at higher energies the background matches ULTRACLEANVETO but with ∼15% more acceptance.

We will work with

P8R3_SOURCE evclass=128
Recommended for most analyses.

Each event class is further divided into **two conversion types**:

- **Front** – conversion in the thin-tungsten layers (better angular resolution)
- **Back** – conversion in the thick-tungsten layers (higher conversion efficiency)

depending on **where** in the Tracker the photon is converted into a $e^+ + e^-$

Event Type	evtype	Description
FRONT	1	Photons converting in the **front section** of the tracker, where the tungsten layers are very thin. These events have **better angular resolution** (narrower PSF) because the electron–positron pair undergoes little multiple scattering, but the probability of conversion is lower.
BACK	2	Photons converting in the **back section** of the tracker, which contains thicker tungsten layers. These events have **poorer angular resolution** due to stronger multiple scattering and bremsstrahlung, but a **higher probability of conversion**.
FRONT + BACK	3	Combination of both FRONT and BACK events. This is the **default choice** in most LAT analyses, since it maximizes photon statistics while accounting for both angular resolution and detection efficiency.

We will **select**

Instrument Response Function

Each event class is associated with a specific Instrument Response Function (IRF). The IRF characterizes how the LAT converts the incoming photon flux from the sky into detected events.

IRF is produced using Monte Carlo simulations

- a large number of γ-rays with different energies and angles is generated
- the photons are propagated through a detailed model of the LAT and its full on- board and ground data processing
- the reconstructed events are compared with the original photons

IRF is the product of three components:

(1) the Effective Area, which describes how efficiently the instrument detects photons

(2) the Point-Spread Function (PSF), which indicates how well the photon direction is determined

(3) the Energy Dispersion, which specifies how accurately the photon energy is reconstructed

LAT reference system

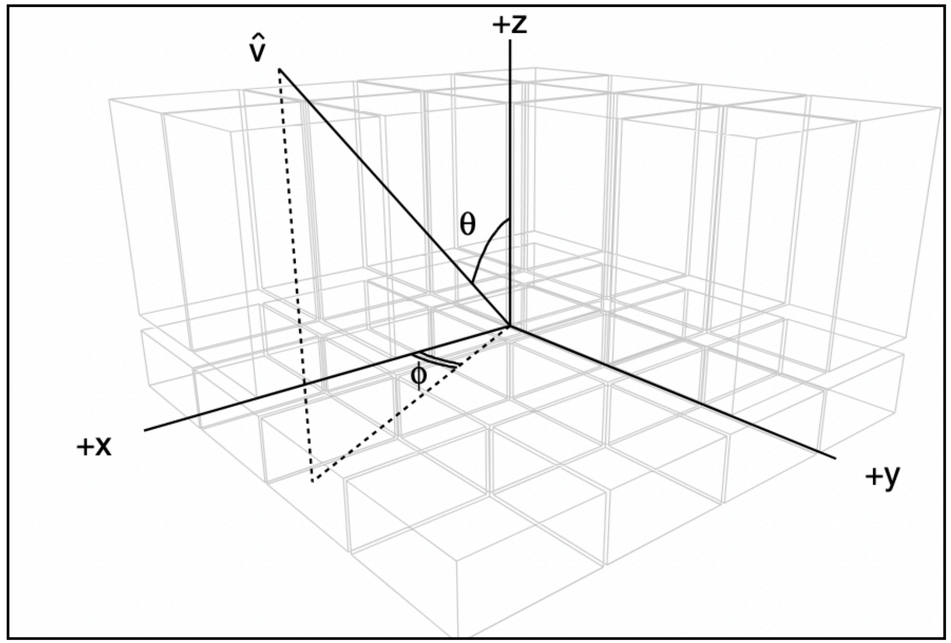

z ->boresight direction (instrument pointing axis)
v -> photon arrival direction described by
θ (incidence angle) and φ (azimuth)

Effective AREA

Aeff (E,v,s), tells us how many γ-rays the LAT can actually detect.

It is obtained by multiplying three factors:

1. **the geometrical area** that the detector presents to the incoming photon,
2. **the probability that the γ-ray converts** into an e/,epair inside the LAT,
3. **the efficiency of the event selection** s, i.e. the probability that the event passes all cuts for that class.

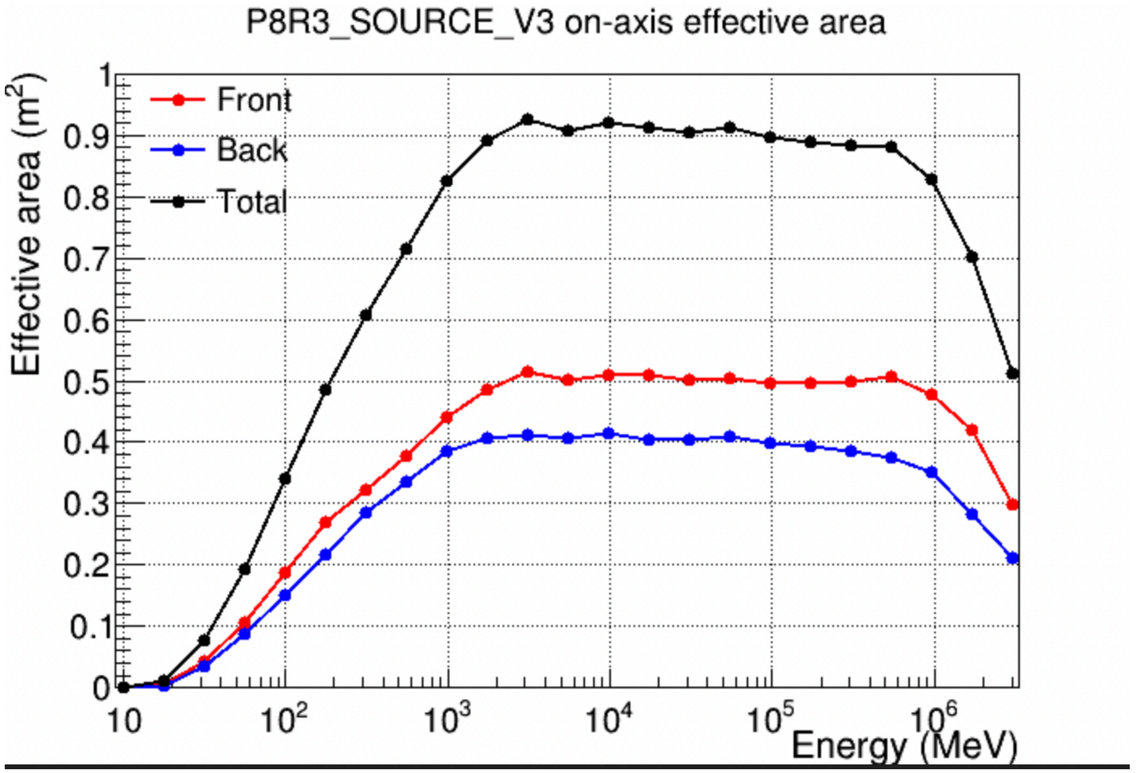

On-axis effective area as a function of the energy

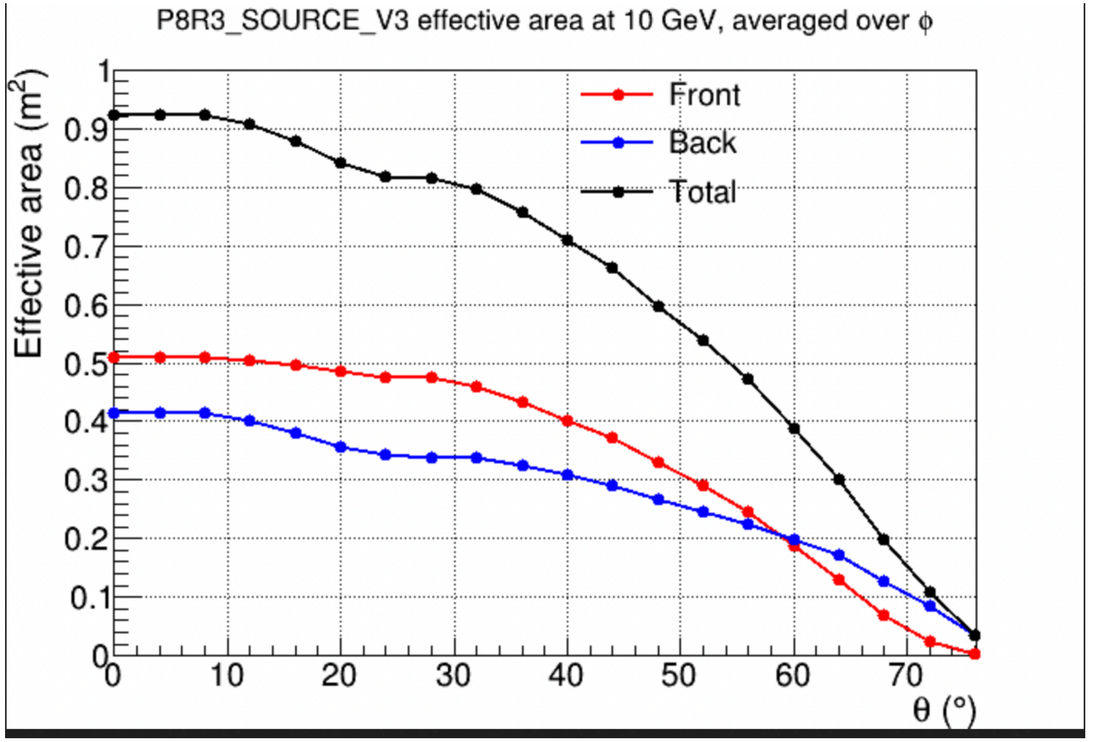

Angular dependence of the effective area at 10 GeV.

The effective are increase up to ~ 1 GeV reflecting $\sigma_{pair} \propto Z^2 \log\left(\frac{E_\gamma}{m_e c^2}\right)$ above ~100 GeV, however, the effective area starts to decrease because photons at these energies convert very efficiently and produce extended electromagnetic showers that may partially escape the detector

As Θ increases, the effective area decreases, reflecting the reduced sensitivity of the instrument for off-axis events.

Acceptance is the integral of the effective area over the solid angle

$$A(E) = \int A_{\rm eff}(E,\theta,\phi)\, d\Omega = \int_0^{2\pi} \int_0^{\pi/2} A_{\rm eff}(E,\theta,\phi)\, \sin\theta\, d\theta\, d\phi,$$

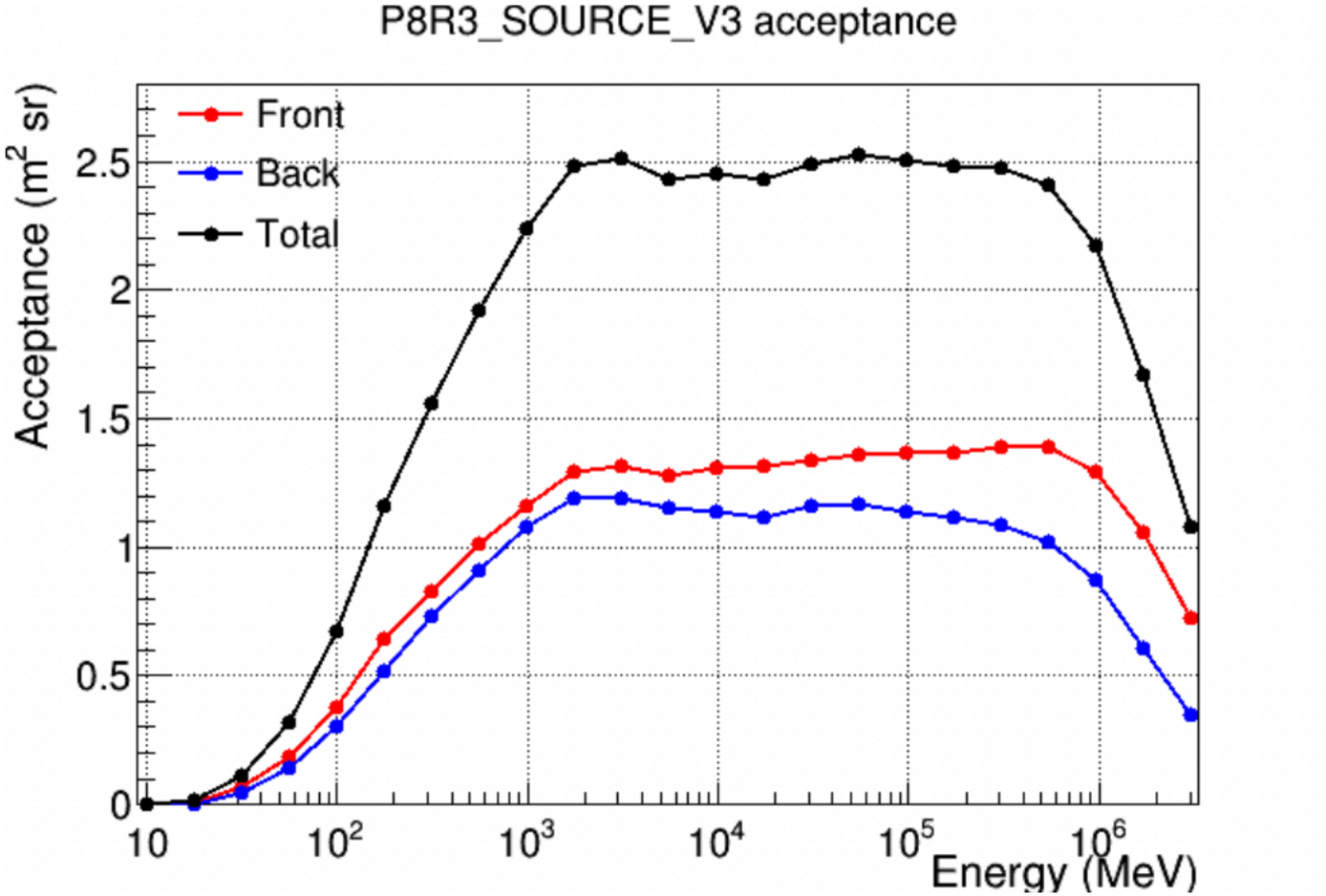

Point Spread Function $P(\hat{v}'; E, \hat{v}, s)$

The Point Spread Function (PSF) describes how accurately the LAT can reconstruct the direction of an incoming γ-ray. It is the probability that a photon with true direction *v* is reconstructed with direction *v'* .

LAT PSF obtained by integrating over all incidence angles and averaging the contribution from each direction, weighted by the effective area.

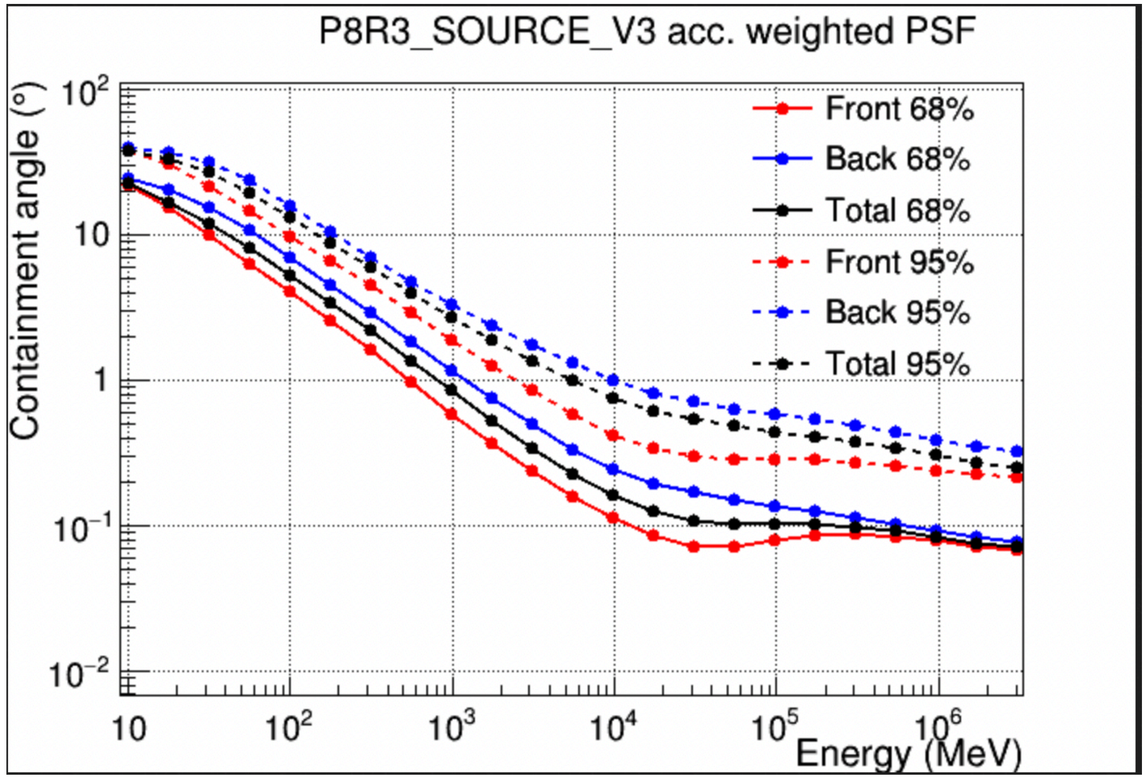

At low energies, the PSF is broad because multiple Coulomb scattering dominates with a deflection angle $\theta \propto \frac{1}{E}$

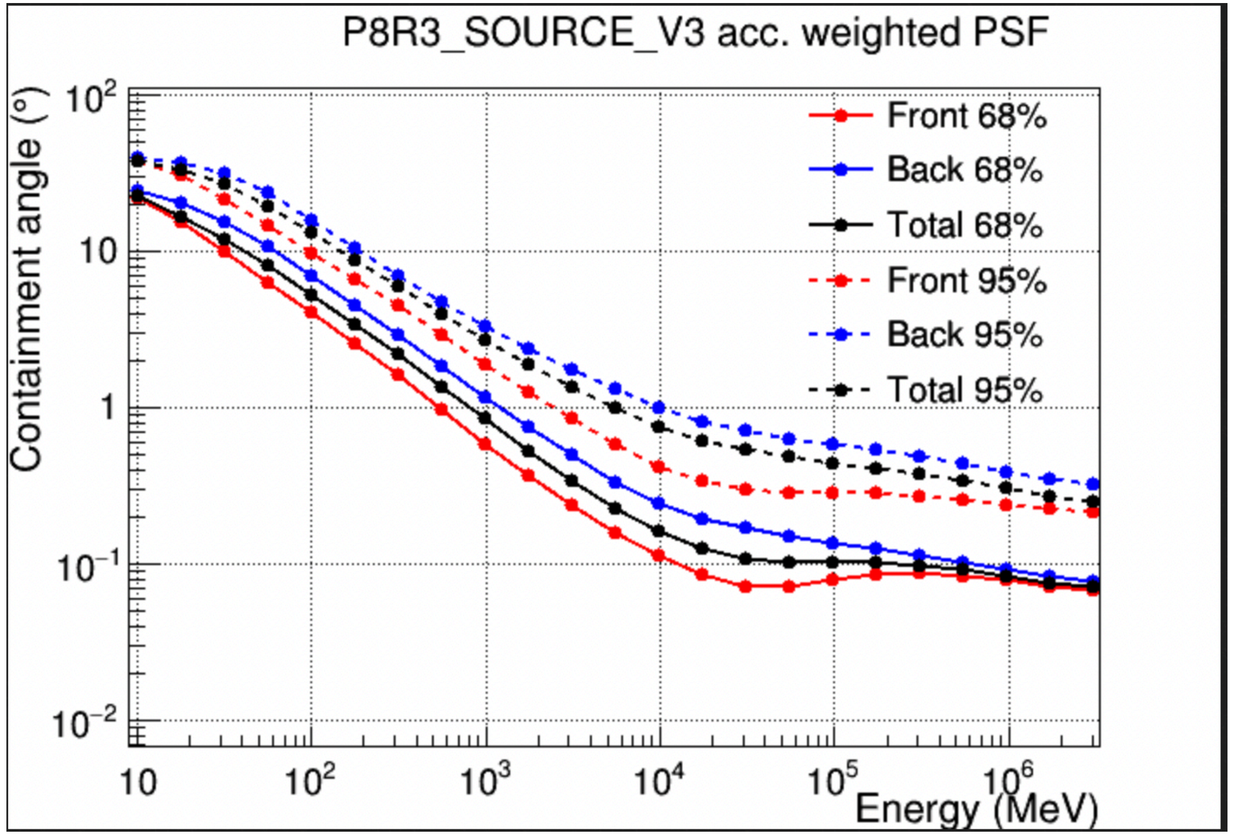

At high energies, scattering becomes negligible and the PSF is instead limited by the tracker spatial resolution.

Energy Dispersion $D\left(E';E,\ \hat{v},\ s\right)$

The Energy Dispersion Function describes how accurately the LAT can measure the energy of an incoming ɣ-ray. It represents the probability that a photon with true energy E is reconstructed with a measured energy E'.

As for the PSF, the final LAT response uses an acceptance--weighted EDF, which averages the results over all incidence angles, giving more weight to directions where the instrument is more efficient and observes longer.

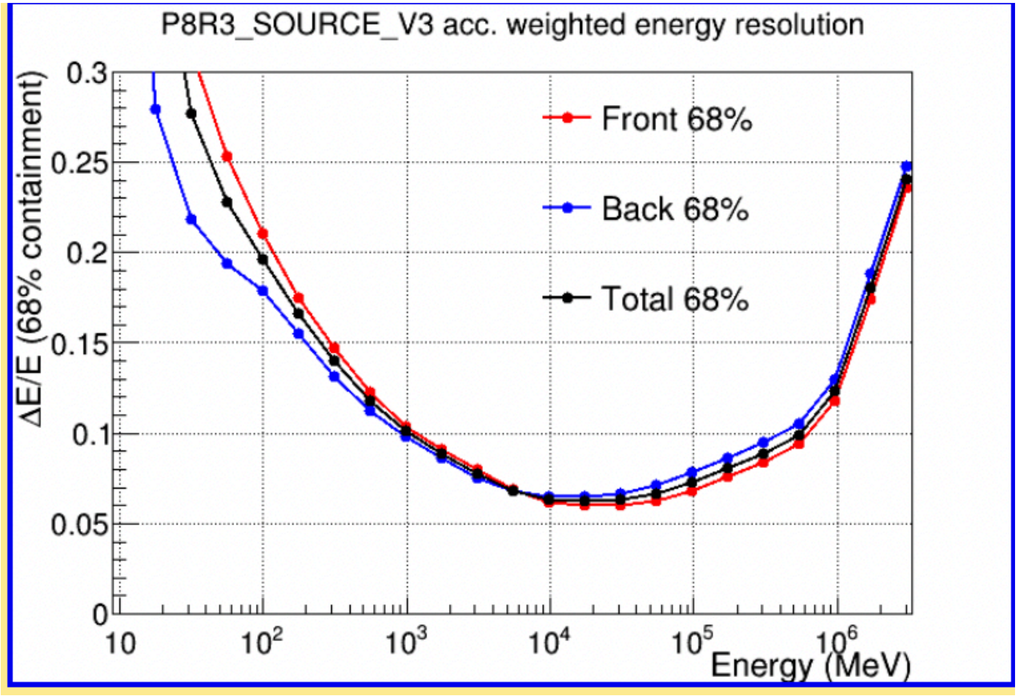

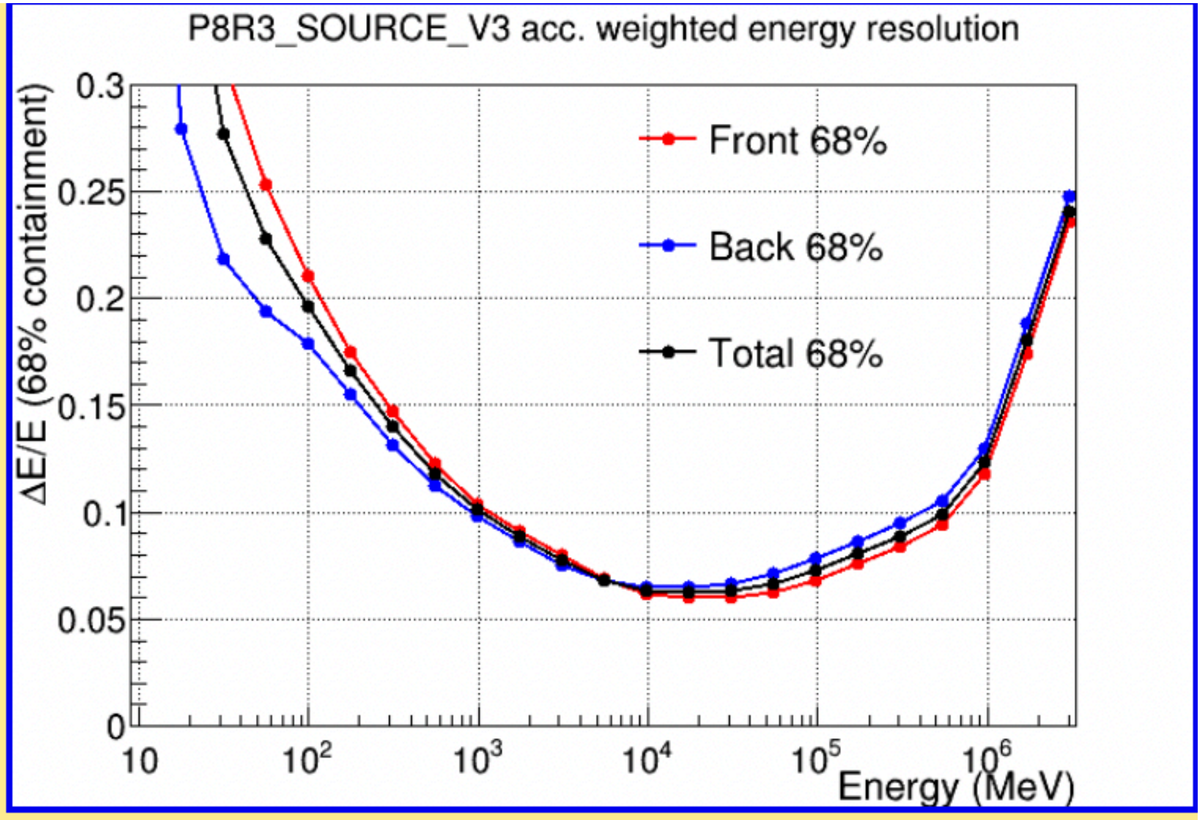

- **Low energies:** the shower is only partially measured → poor resolution.
- **Intermediate energies:** the shower is well contained → best resolution.
- **High energies:** part of the shower leaks out of the calorimeter → resolution worsens again.

Which statistics do we use in gamma rays?

In gamma-ray astronomy, the number of detected photons is often very small.

- Gaussian approximation is valid for a large number of counts per energetic bin (typically at least 15–20)

Gaussian statistics cannot be used in the gamma-ray regime

LIKELIHOOD ANALYSIS

THE LIKELIHOOD **L** IS THE PROBABILITY OF OBTAINING YOUR DATA GIVEN AN INPUT MODEL. BY MAXIMIZING **L** WE FIND THE MODEL PARAMETERS THAT BEST MATCH THE OBSERVED DATA.

If the model predicts an average number of counts m_i in the i-th bin, and the data contain n_i observed counts, the probability of observing n_i is

$$p\left(n_i\right) = \frac{m_i^{n_i}}{n_i!}\, e^{-m_i}.$$

The likelihood L is the product of these probabilities for all bins:

$$L = \prod_i \frac{m_i^{n_i}}{n_i!}\, e^{-m_i}.$$

The exponential factors can be combined,

$$\prod_i e^{-m_i} = e^{-\sum_i m_i} = e^{-N_{\rm exp}},$$

where $N_{\rm exp}$ is the total number of events predicted by the model. Thus the likelihood becomes

$$L = e^{-N_{\rm exp}} \prod_i \frac{m_i^{n_i}}{n_i!},$$

and taking the logarithm gives

$$\log L = -N_{\rm exp} + \sum_i n_i \log\left(m_i\right) - \sum_i \log\left(n_i!\right).$$

How do we apply the likelihood in the case of the Fermi-LAT?

- The sky model contains all gamma-ray sources that contribute to the Region of Interest (ROI), together with the diffuse background components.
- These model components are then folded with the Instrument Response Functions (IRFs) to predict the number of detected events.
- The likelihood is maximized by varying the model parameters until the best agreement with the data is reached.

Total Sky Model in the ROI

Model components in the ROI

The total model in the ROI is the sum of all point-like or extended sources plus the diffuse background components:

$$S_{\rm tot}\left(E,\hat{p}\right) = \sum_{i=1}^{N} S_i\left(E,\hat{p};\eta_i\right) + \beta_{\rm gal}\, B_{\rm gal}\left(E,\hat{p}\right) + \beta_{\rm iso}\, B_{\rm iso}\left(E\right).$$

Total Model

All the sources in the ROI

Background

Components:

- $S_i\left(E,\hat{p};\eta_i\right)$: spectral and spatial model of source i;
- $B_{\rm gal}$: Galactic diffuse emission (normalization $\beta_{\rm gal}$);
- $B_{\rm iso}$: isotropic diffuse emission (normalization $\beta_{\rm iso}$).

The parameter vector for each source is

$$\eta_i = \{\text{normalization},\ \Gamma,\ E_{\rm cutoff},\ \text{extension},\ldots\}.$$

Predicted Counts: Folding the Model with the IRFs

The total sky model cannot be compared directly with the detected events. Instead, it must be folded with the IRFs, which include the effective area, the point-spread function (PSF), the energy dispersion, and the time-dependent spacecraft orientation.

The predicted number of detected counts in reconstructed energy E', reconstructed direction $\hat{p}'$, and event type s is given by

Predicted events

$$M\left(E', \hat{p}', s\right) = \iiint S_{\mathrm{tot}}\left(E, \hat{p}\right) R\left(E', \hat{p}', s; E, \hat{p}, t\right) dE\, d\Omega\, dt.$$

IRF

For a binned analysis, the expected counts in bin k are

$$m_k = \int_{\mathrm{bin}\ k} M\left(E', \hat{p}', s\right)\, dE'\, d\Omega'.$$

The Likelihood Function

Assuming Poisson statistics for the number of detected events in each bin, the likelihood comparing predicted counts m_k with observed counts n_k is

$$\mathcal{L}\left(\{\theta_i\}, \beta_{\mathrm{gal}}, \beta_{\mathrm{iso}}\right) = \prod_k \frac{m_k^{n_k} e^{-m_k}}{n_k!}.$$

The best-fit parameters maximize the likelihood:

$$\{\theta_i^*,\ \beta_{\mathrm{gal}}^*,\ \beta_{\mathrm{iso}}^*\} = \arg\max_{\theta_i, \beta_{\mathrm{gal}}, \beta_{\mathrm{iso}}} \mathcal{L}.$$

I. SKY MODEL IN THE ROI

Model=(all sources)+(diffuse background)

(Source model depends on several parameters(e.g. normalization, background on normalization

II. MODEL FOLDED WITH THE IRFs

M=Model⊗IRFs

(IRFs = PSF, Effective Area, Energy Dispersion)

II. TOTAL PREDICTED NUMBER OF COUNTS

$$N_{\rm pred} = \sum_{\rm ROI} M$$

IV. EXPECTED COUNTS IN BIN k

$$N_{\rm pred} = \sum_{\rm bin\ k} M$$

See slide 17

Illustrative Example of the Likelihood

Summary

In summary, applying the likelihood method to Fermi–LAT data involves:

(1) building a sky model including all sources and diffuse components;

(2) folding this sky model with the IRFs to predict the detected counts;

(3) comparing predicted and observed counts with a Poisson likelihood;

(4) varying the source and background parameters until the likelihood is maximized.

This procedure yields the parameter values that best describe the gamma-ray data in the ROI.

In Fermi-LAT analyses, the detection of a γ-ray source is based on the likelihood ratio test. The null hypothesis H_0 corresponds to a sky model in which the source is not included, while the alternative hypothesis H_1 includes the source with one or more free parameters such as the flux normalization and, possibly, the spectral index. For each hypothesis we compute the maximum likelihood of the observed photon data assuming Poisson statistics. The Test Statistic (TS) used by the LAT is defined as

$$TS = -2 \ln \left(\frac{L_0}{L_1} \right) = 2 \left(\ln L_1 - \ln L_0 \right),$$

where L_0 and L_1 are the maximized likelihoods under H_0 and H_1. A large value of TS indicates that the inclusion of the source in the sky model provides a significantly better description of the data.

The interpretation of TS relies on *Wilks' theorem.* This theorem states that when two statistical models are *nested* — that is, when the more complex model H_1 reduces to the simpler one H_0 by imposing q constraints on its parameters — the likelihood-ratio statistic

$$-2 \ln \left(\frac{L_0}{L_1} \right)$$

converges in distribution to a chi-square distribution with q degrees. Therefore, if only the normalizzation (k) of a power law model ($F(E) = kE^{\Gamma}$) for example is let free to vary, the LAT detection statistic is asymptotically distributed as

$$TS \sim \chi^2_1$$

and the detection significance can be approximated by

$$\text{Significance} \approx \sqrt{TS},$$

The source

The blazar **TXS 0506+056** <(z = 0.336500) is the most well-known case in which a neutrino emission has been associated with an astrophysical source.

- The neutrino event is identified as **IceCube-170922A**, detected on September 22, 2017 by the IceCube Neutrino Observatory, with an energy of about 290 TeV.
- In the direction of the neutrino, TXS 0506+056 was in a **gamma-ray flaring state**, allowing a spatial and temporal association.
- This is considered the first high-energy astrophysical neutrino source identified with a good level of confidence.

More information on tithes source can be found here

JOURNAL ARTICLE

TXS 0506+056, the first cosmic neutrino source, is not a BL Lac FREE

P Padovani ✉, F Oikonomou, M Petropoulou, P Giommi, E Resconi

Monthly Notices of the Royal Astronomical Society: Letters, Volume 484, Issue 1, March 2019, Pages L104–L108, https://doi.org/10.1093/mnrasl/slz011

Published: 23 January 2019 **Article history** ▾